Supplementary Information for

Identifying and controlling the order parameter for ultrafast photoinduced phase transitions in thermosalient materials

S. Ghasemlou, X. Li, D. Galimberti, T. Nikitin, R. Fausto, J. Xu, S. Holleman, T. Rasing, H.M. Cuppen

E-mail: h.cuppen@science.ru.nl

This PDF file includes:

Other supplementary materials for this manuscript include the following:

Supporting Information Text

Molecular dynamics simulations of the stable forms

Molecular dynamics simulations of the α and β forms were performed to obtain information on several structural properties of the stable forms. These can be observed in Figure S1a and b for α and β, respectively. A pre-equilibrated structure was simulated at 400 K for 500 ps in the case of the α structure and 450 K for the β structure. For both simulations, simulation cells of $8 \times 1 \times 8$ crystallographic units were used, which corresponds to cells with roughly equal sizes of approximately 50 Å. The figure shows crystallographic lattice parameters a, b, and c as well as the a/c ratio which sensitively changes during the phase transition. The bottom two panels show the average value of the dihedral angles θ and ϕ, whereas the colored region accounts for the standard deviation in these angles.

The simulations show that the dihedral angles θ and ϕ fluctuate around stable values, which are different for the α and β forms and which are in good agreement with the values obtained by X-ray diffraction (see Table 1). However, the dispersion for individual angles is rather large as can be seen from the purple areas in Figure S1. Both large dynamic fluctuations, where the individual angles change rapidly in time (not shown here, but visible in Fig. 4 of (1)), and large static fluctuations, with a broad angular distribution at any given time (indicated by the light purple areas), were observed. This distribution appears larger for the β form than for the α form, even corrected for the temperature difference.

Molecular Dynamics simulations of spontaneous transitions

Unbiased simulations of the α phase were performed during which the simulation cell is heated. This is shown in Figure S2a. Here the cell is initially kept at 400 K for 100 ps, the cell is then heated to 450 K for the next 100 ps, and for the remainder of the simulation, the cell is kept at this temperature. The figure shows that the dihedral angle ϕ decreases and the fluctuations in the angle increase during the warm-up phase. The cell dimensions and dihedral angles then remain roughly constant until 300 ps. Then, there is an initial change in angle ϕ and axes a and c at this time. The dihedral θ remains constant and the transition does not continue. At 340 ps a full transition starts which takes roughly 20 ps to proceed. Figure S2b shows the reverse transition. Here the β form is cooled down from 450 K to 400 K. Here we see that the transition already starts during the cool-down phase. It appears that the transition takes slightly longer and the change in cell lengths, and dihedral angles is not as fast as for the reverse direction. This can be because of the slightly lower temperature at which the transition occurs.

The unbiased simulations further confirm the inclusion of both θ and ϕ angles in our order parameter. Initial changes in either θ and ϕ are observed, but these do not lead to a transition unless both angles change simultaneously. This can be seen in Figure S2 and is also observed in duplicate simulations with the same settings but different initial conditions. If a constructed collective variable does not capture the true reaction coordinate, this will lead to an overestimation of the free energy barrier. The fact that the free energy barrier is observed to disappear as a function of temperature is another indication of the suitability of the collective variable s as the order parameter describing the α to β phase transition.

Figure S3 shows the (a, c) in-plane nucleus size of the β form as a function of time during the trajectory belonging to Figure S2a. The nucleus size is determined by the θ angle of the molecule. Each biphenyl segment is classified belonging to either α or β using kmeans classification based on θ. Segments that are neighbors in the (a, c) plane and that are both classified as β are considered to be part of the same nucleus. Since only in-plane neighbors are considered the maximum cluster size is 128. Each simulation cell contains four layers of segments in the (a, c) plane. The colored squares in Figure S3 indicate the θ angles for those four layers at three different times. Initially some clusters of β exist. These fluctuate in size, as can be seen between 300–320 ps. At 337 ps, most segments are in the α configuration, indicated by the abundance of blue. It can be seen that segments orient depending on their neighbors, although the correlation length is small. No correlation would lead to a completely random distribution of the different blue tones. Around 340 ps the β clusters can be seen to grow in size. This goes gradually over 10 ps. The snapshots at 345 ps shows areas of red clusters, again indicating some correlation between immediate neighbors, but no long-range collective effect. The observed behavior is in agreement with either a nucleation-and-growth mechanism or a phonon-like/wave-like transition with a short wavelength of a few molecules wide ($\sim$ 10 Å) which should correspond to a frequency in the terahertz range. A collective displacive mechanism where all molecules transform simultaneously would have resulted in a more binary nucleation-size graph, where the full layer is simultaneously transformed to β, without the intermediate cluster sizes and more homogeneously colored snapshots.

Convergence of the metadynamics simulations

Figure S4 shows the time evolution of s, θ, and ϕ during a metadynamics simulation at 400 K. Both α and β phase are visited multiple times. To converge the free energy profile the height of the added hills is reduced at several times, as indicated by the dashed lines.

Figure S5 shows the free energy profiles of the $\alpha \leftrightarrow \beta$ transition at 400 K for different simulation cell sizes. The free energy is given per molecule in the simulation cell. Since the free energy is an extensive property, this should result in similar ΔF for all simulations. This is indeed the case for the simulations which are larger than $a \times c = 4 \times 4$. For the two cells with $a \times c = 4 \times 4$ the finite-size effect likely results in a different ΔF between the α and β form and this is an artifact of the simulation. The $\beta \rightarrow \alpha$ free-energy barrier does not necessarily scale with simulation size, but the resolution of the metadynamics simulations is not high enough to be conclusive on this point.

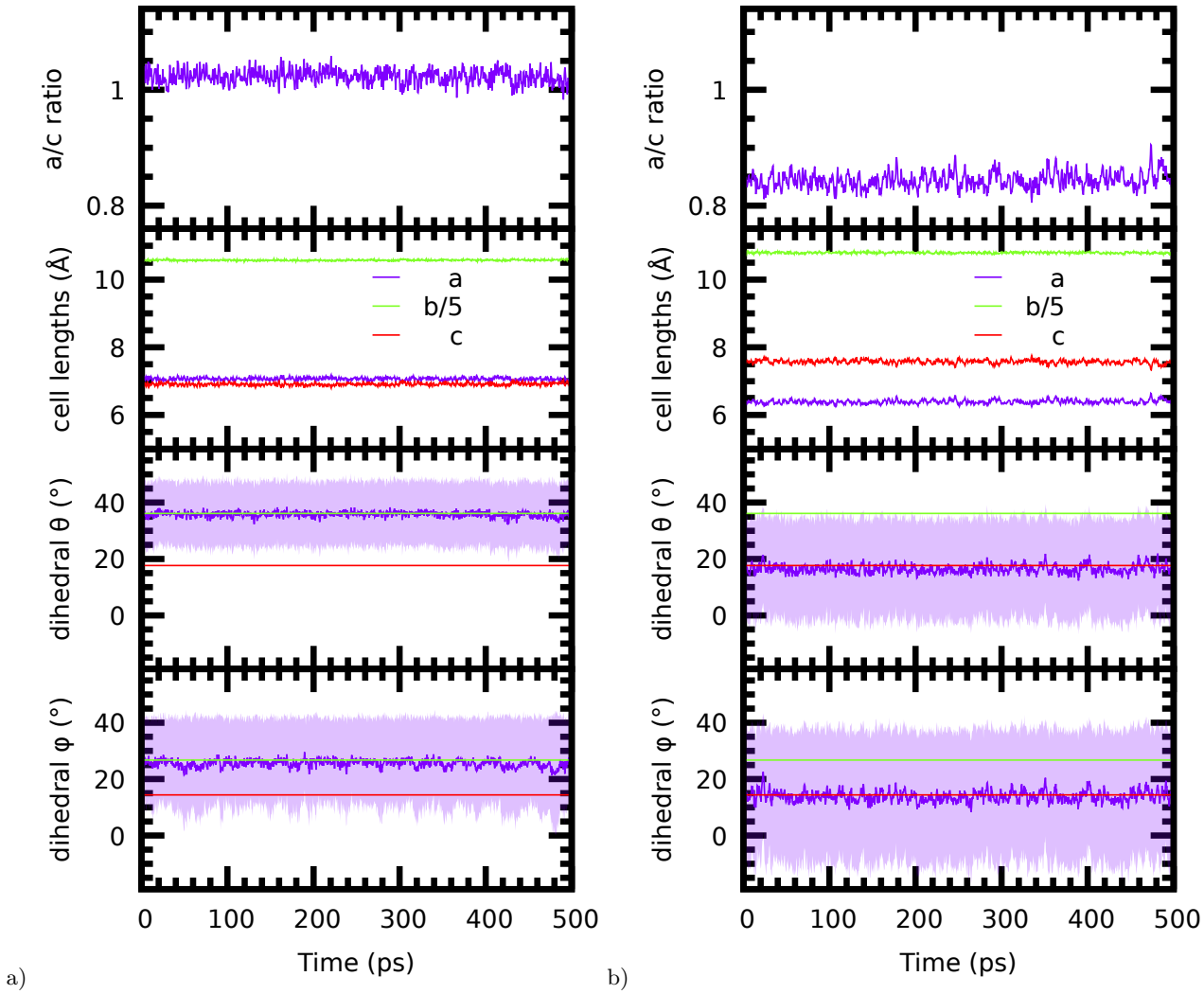

Fig. S1. Structural parameters of the a) α form at 400 K and b) β form at 450 K as obtained by MD simulations. A simulation cell of $8 \times 1 \times 8$ unit cells is used.

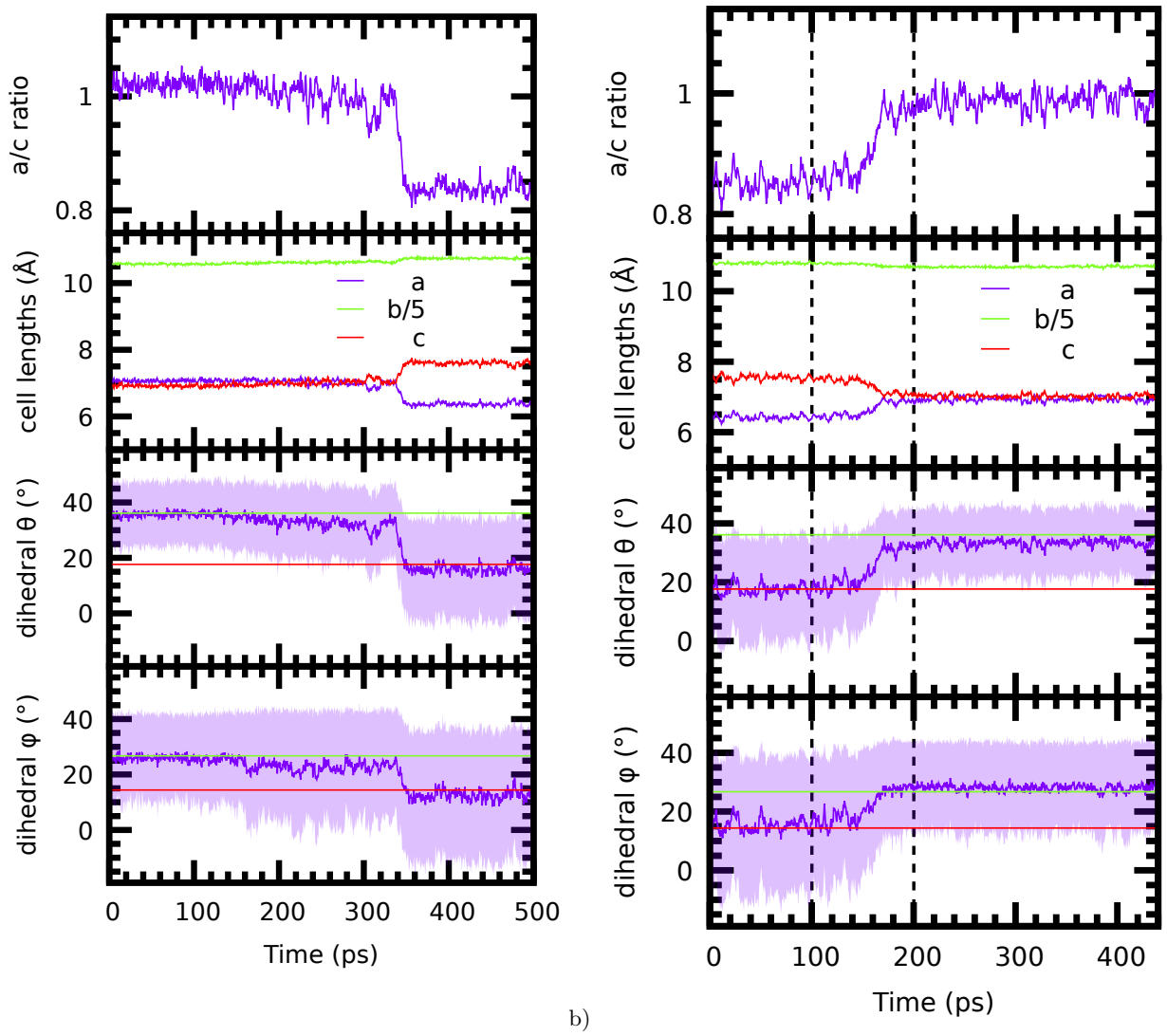

Fig. S2. a) Heating of an $8 \times 1 \times 8$ simulation cell of the α from 400 K to 450 K, b) cooling of $8 \times 1 \times 8$ β cell from 450 K to 400 K, c The heating or cooling starts at 100 ps and ends at 200 ps after which the temperature is kept constant.

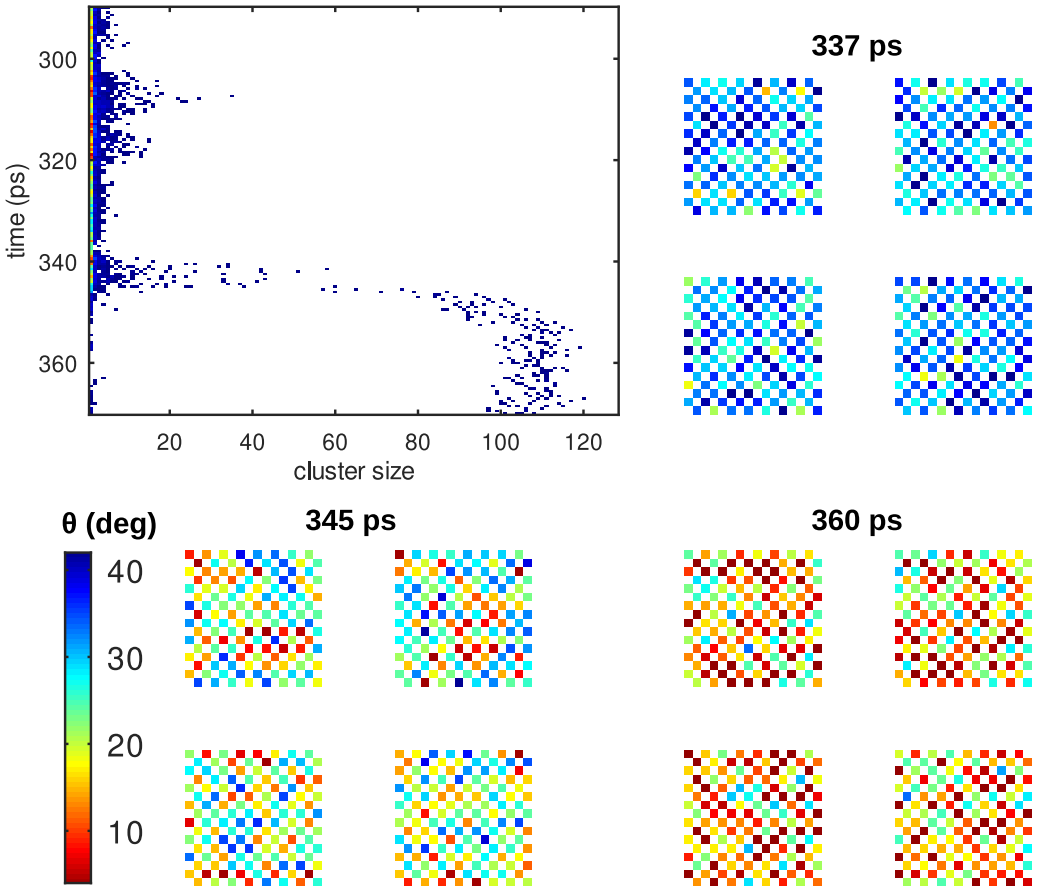

Fig. S3. In-plane nucleus size of the β form during the trajectory belong to Figure S2a. The maximum cluster size is 128.

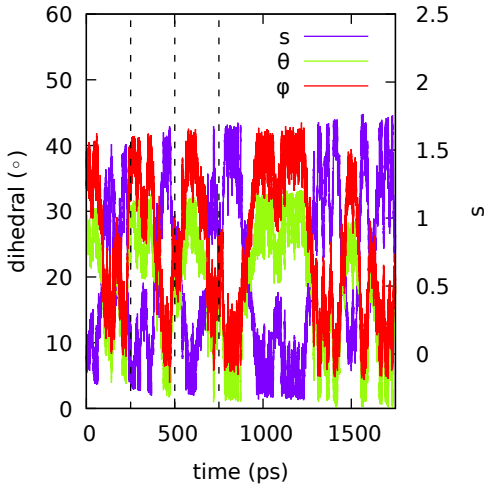

Fig. S4. Time evolution of s, θ, and ϕ during a metadynamics simulation at 400 K. The height of the hills is reduced by a factor of two at each dashed vertical line.

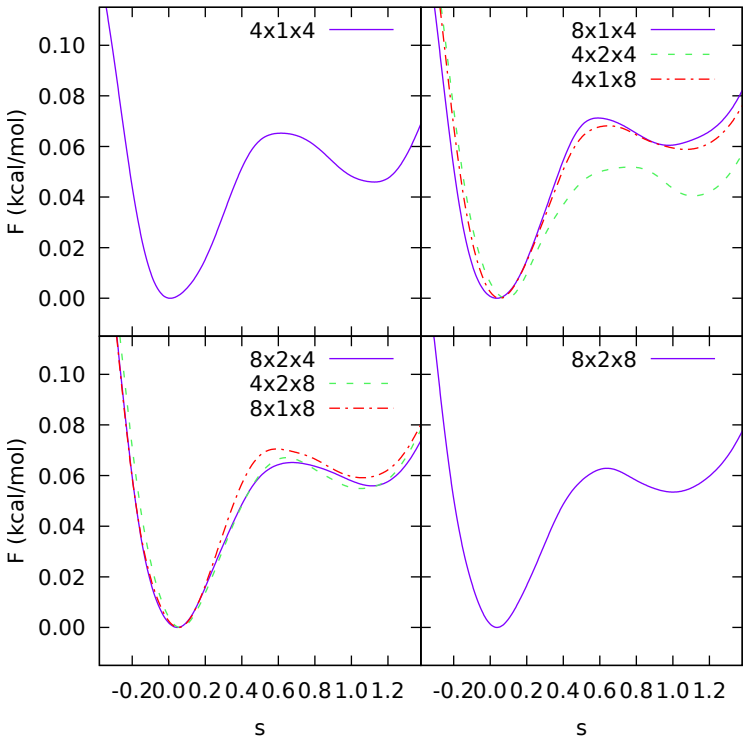

Fig. S5. Free energy profiles of the $\alpha \leftrightarrow \beta$ transition at 400 K for different simulation cell sizes. The free energy is given per molecule in the simulation cell. Cells with the same number of molecules are in the same panel. Curves have been shifted to match $G(s = 0) = 0$.

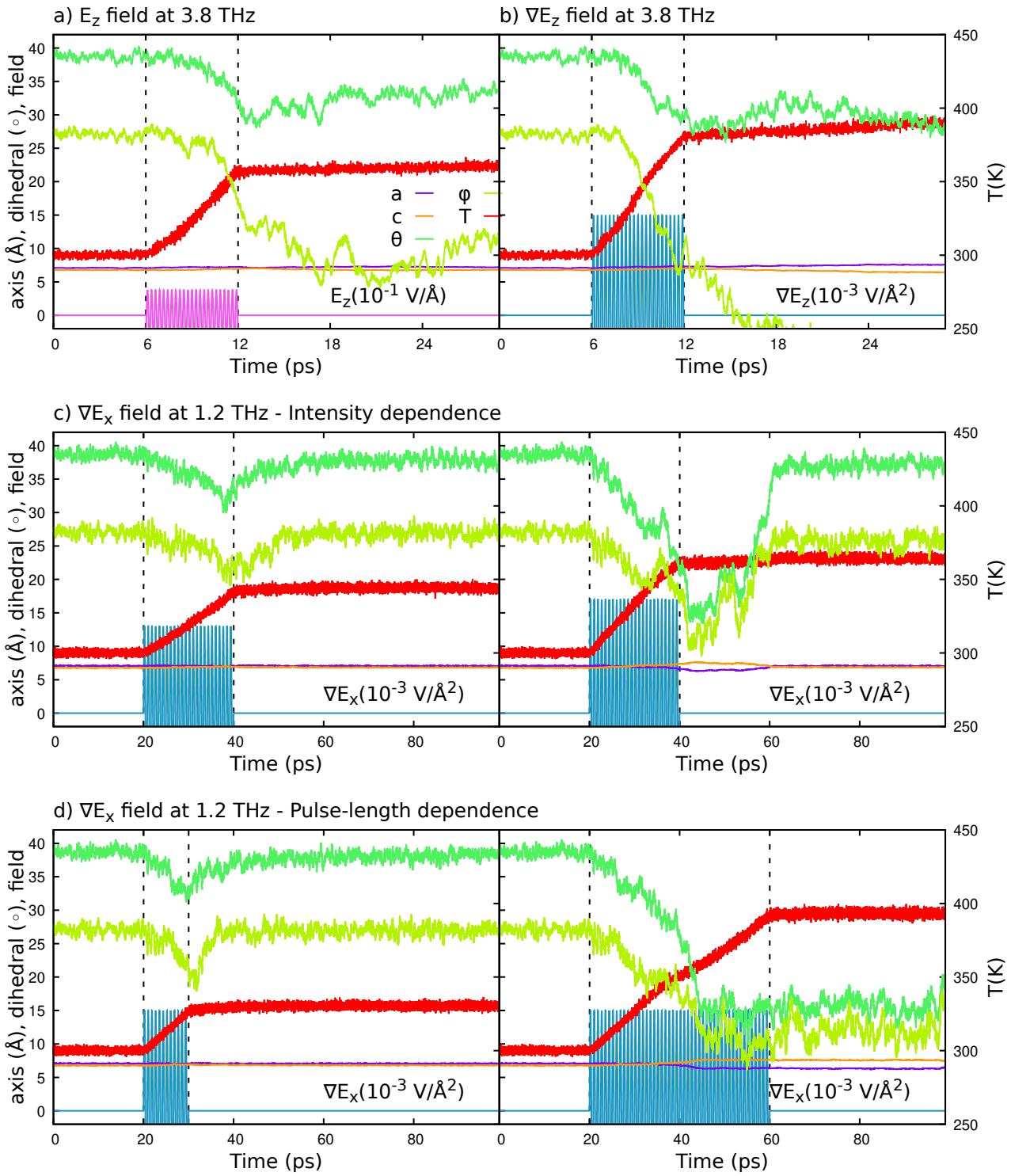

Fig. S6. Dependency of the triggered phase transition on a) + b) frequency, c) duration, and d) intensity of the pump pulse. In a), c) and d) a quadrupole field is applied, and in b) an electric/dipole field. Shown are the structural parameters a, d, θ, and ϕ, the applied field strength, and the temperature of the system T. The simulation cell is initialized at $T = 300$ K.

Ultrafast photoinduced phase transition

Movies of the trajectories that resulted in structural changes upon a field are part of the Suppl. Information. Higher resolution versions can be found through https://doi.org/10.34973/j5ax-am79. The phenyl rings in these movies are colored according to their dihedral angle and the direction of the field gradient is parallel to the field of view.

The trajectory belonging to Fig 4b shows that an initial nucleus is formed that propagates across the system. Along with the rotation of the rings, a change in the distance between the molecules occurs, consistent with the change in lattice parameters. This is confirmed by the trajectory belonging to Fig. S6d-right, which has an electric field gradient with higher intensity.

Figure S6a and b illustrate the dynamic behavior of the system upon exciting the mode around 3.8 THz, applying an electric field and an electric field gradient pulse along z, respectively. Pulses along x and y resulted in limited adsorption of energy and no structural changes, similar to Figure 4a. The orange line indicates the pulse again. In both panels, the pulse triggers an increase in temperature (red), followed by changes in the dihedral angles. However, for this pulse the main change is in ϕ, corresponding to only outer ring rotation, while the pulse at 1.2 THz resulted in simultaneous changes in both θ and ϕ, immediately followed by changes in a and c. At 3.8 THz, the lattice axes remain rather unaffected and θ only changes after some time delay and recovers again. The corresponding trajectories show that indeed at 3.8 THz only the rotations of the rings are triggered, without the additional changes in distance between the molecules and the corresponding phase transition. Figure S7 confirms that there is indeed an infrared-active mode present at 3.8 THz.

We would like to note that the applied electric field in Figure 4a is nearly two times larger than the field in Figure S6a, thus the lack of adsorption at 1.2 THz is not due to a too low electric field intensity, but because the transition is not IR-active, as confirmed by the calculated IR spectra in Figure S7.

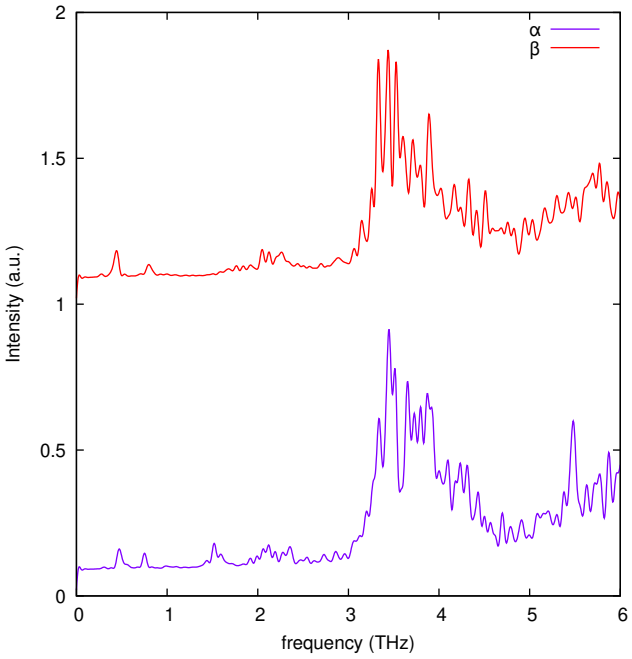

Fig. S7. Calculated IR spectrum for the α and β form at 425 K.

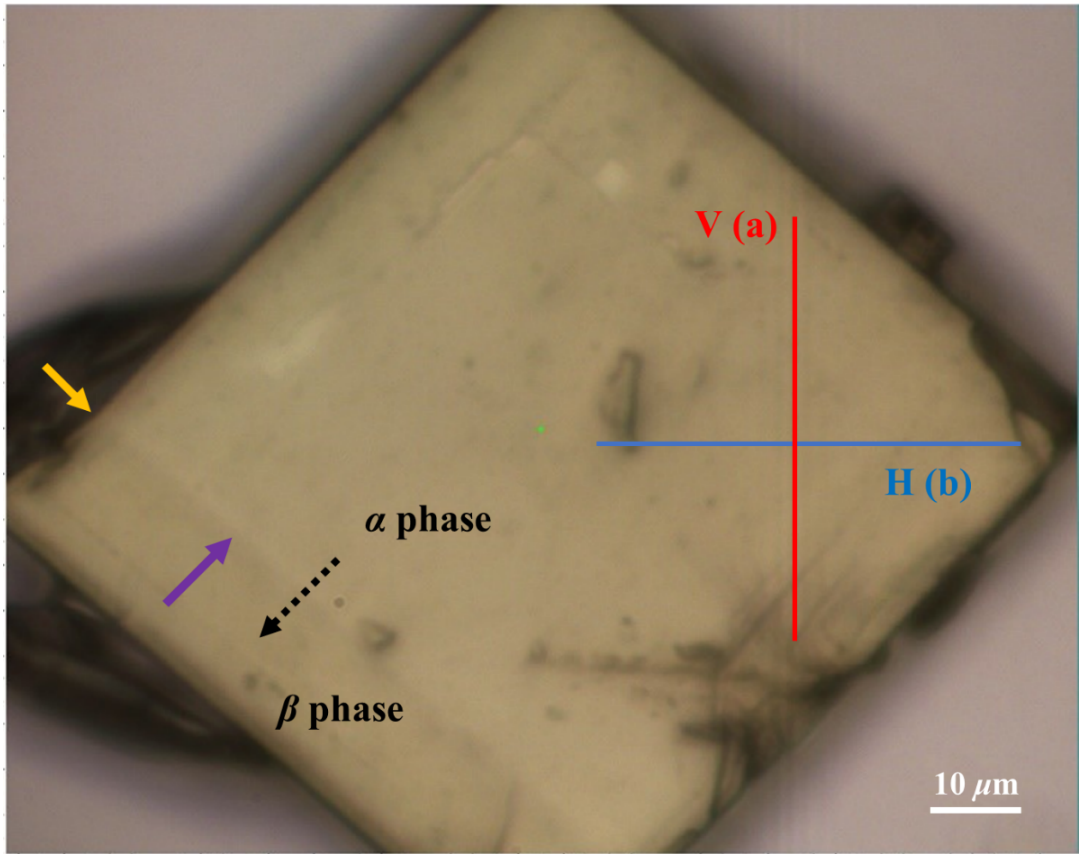

Fig. S8. Shape transformation and phase boundary propagation of 4-DBpFO single crystal upon heating. The vertical and horizontal polarizations are denoted with red and blue lines, which are parallel to the crystallographic a- and c-axis respectively. A phase boundary appears from the bottom left edge, and remains fixed at a temperature of 182.5 °C. The yellow arrow points out the fixed position of the phase boundary whereas the purple arrow points into the propagation direction of the phase boundary upon increasing temperature. The black arrow indicates the line scan measurement direction from the α to the β phase.

Movie S1. pump-1.2THz-0.015-x.mp4: This trajectory belongs to Fig 4b.

Movie S2. pump-1.2THz-0.015-w2-x.mp4: This trajectory belongs to Fig. S6d-right.

Movie S3. pump-3.8THz-0.38-z.mp4: This trajectory belongs to Fig. S6a.

Movie S4. pump-3.8THz-0.015-z.mp4: This trajectory belongs to Fig. S6b.

Additional data table S1 (alpha-264.data)
LAMMPS data file for a single unit cell of the α form

Additional data table S2 (beta-265.data)
LAMMPS data file for a single unit cell of the β form

References

1. Y. Duan, S. Semin, P. Tinnemans, H. M. Cuppen, J. Xu, and T. Rasing. Robust thermoelastic microactuator based on an organic molecular crystal. *Nature Comm.*, 10:4573, 2019. .